ATLAS Internal Note
CAL-NO-021
7 June 1993

Study of the effect of the radiation on a TILECAL hadron calorimeter intended to be used in the ATLAS Experiment on the Barrel region

A. Amorim[1], A.Henriques[2], A. Maio[1]
(RD34 Collaboration)

Abstract

The effects of radiation damage induced by neutrons and charged particles on the performance of a TILECAL Barrel hadron calorimeter are studied. For an integrated luminosity of $10^6 pb^{-1}$ (10 years running at a peak luminosity of $1.6x10^{34}cm^{-2}s^{-1}$) the degradation on the jet energy resolution and the light reduction are marginal, even when the 4 longitudinal sectors of the calorimeter are not periodically recalibrated. The largest effect is observed in the light reduction on the first tile, starting at 1.95λ, which is 6.2% at $\eta = 1.5$ and 4.8% at $\eta = 0$. At $\eta = 1.5$, the most exposed region in the Barrel region, the increase on the jet energy resolution of 300 GeV incident jets is 0.24% without longitudinal calibration and 0.16% when the calibration is applied. The signal is reduced by 1.51% without calibration and 0.14% after calibration.

I) Dose Levels Expected in the Barrel Hadron Calorimeter in ATLAS.

The doses given below are taken from the ATLAS LoI (pag. 81) and from the A. Ferrari presentation in the calorimeter working group in July 1992 (CAL-TR-059). They include the dose coming from charged particles and neutrons, considering a mean medium in the calorimeters (LAr/Pb in the e.m. calorimeter and LAr/Iron in the had. calorimeter).

In Fig.1 are given the isodose curves expected in the ATLAS detector per year for an integrated luminosity of 10^5 pb^{-1}. The step between two isodose curves is 5 Gy, see also table 1. The doses expected in the hadron Barrel calorimeter are given in more detail in fig. 2. The curves drawn on the lego plot correspond to the doses for $\eta = 0$ and $\eta \approx 1.5$ as a function of the calorimeter depth, with peak doses of 10 Gy/yr and 20 Gy/yr respectively.

Detector Component	Dose	Neutron Flux	
	(kGy y^{-1})	with mod. (cm^{-2} y^{-1})	no mod. (cm^{-2} y^{-1})
SITV	28	6.0×10^{12}	2.5×10^{13}
SIT	1.6	1.9×10^{12}	1.9×10^{13}
End-cap TRDs	4.0	3.4×10^{12}	2.8×10^{13}
Barrel *em* calorimeter	0.4	6.8×10^{12}	1.7×10^{13}
Barrel hadron calorimeter	0.02	1.0×10^{12}	1.4×10^{12}
End-cap *em* calorimeter	21	8.2×10^{13}	9.1×10^{13}
End-cap hadron calorimeter	4.0	4.0×10^{13}	5.1×10^{13}
Forward calorimeter	830	1.1×10^{15}	

Table 1- Peak neutron fluxes (for $E_n \geq 100$ keV) and doses of the ATLAS detector components with and without a 5 cm polyethylene layer in front of the calorimeters [ATLAS LoI, pag. 81]. This simulation was done considering a Pb/LAr e.m. calorimeter and a Fe/LAr had. calorimeter.

1- LIP and University of Lisbon, Lisbon, Portugal.
2- CERN, Geneva, Switzerland.

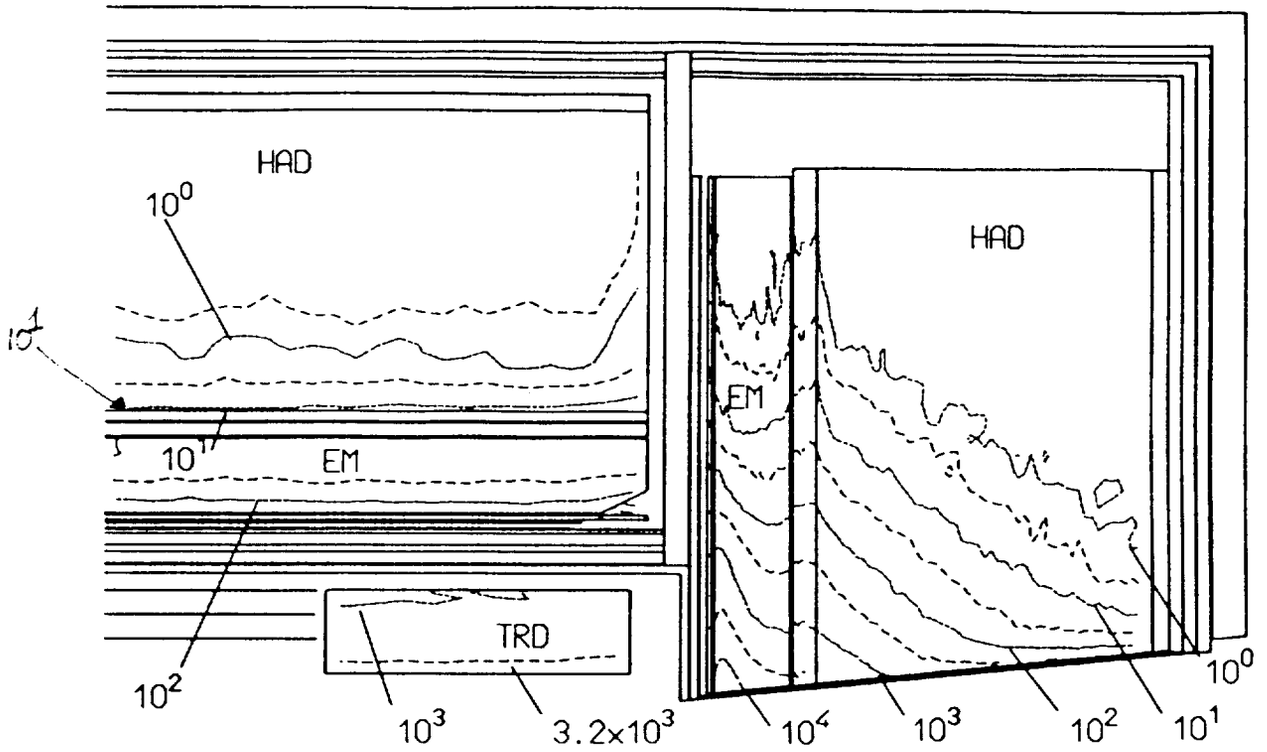

Fig. 1 Lines of constant radiation doses in Gy/y for a yearly integrated luminosity of $10^5 pb^{-1}$ [ATLAS Loi, pag. 81].

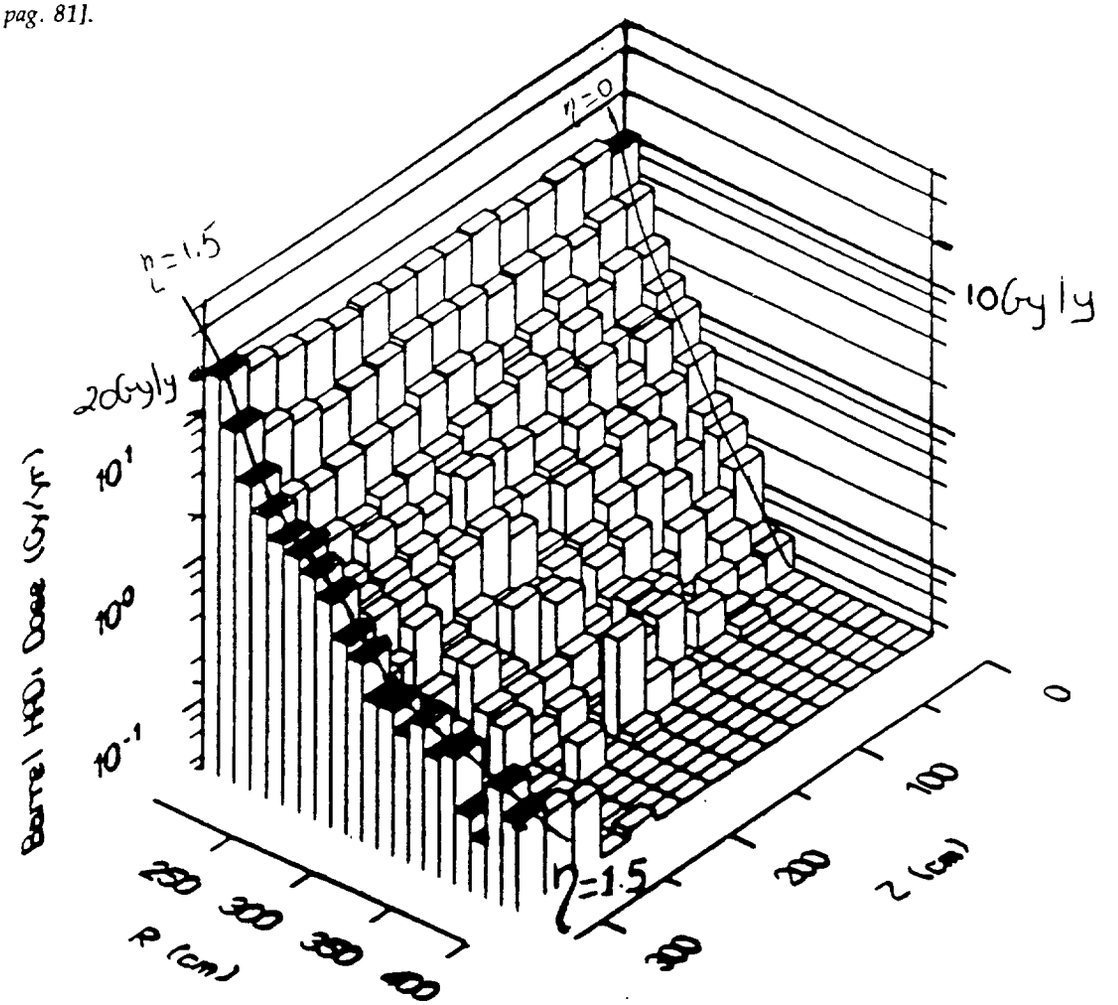

Fig. 2- Doses expected in the hadron barrel calorimeter [Ferrari, CAL-TR-059]. The lines give the doses expected for $\eta = 0$ and $\eta \approx 1.5$ for a yearly integrated luminosity of $10^5 pb^{-1}$.

Corrections applied to the dose in the case of a TILECAL Hadron Calorimeter

There are some corrections to be applied to the expected dose in the case of a Hadronic TILECAL calorimeter. The contribution of the neutron fluxes and charged particles to the total dose given above by Ferrari et al. have been calculated considering a mean medium of absorber and active material. In the case of a iron/plastic scintillator calorimeter with a ratio of 4.5 to 1, the dose induced by neutrons and charged particles in the plastic scintillator is higher and has to be corrected for.

Corrections applied to the doses induced by neutrons

In the development of a hadronic shower a fraction of the energy spent in the form of nuclear excitation (binding energy loss) appears in the form of slow neutrons after nuclear deexcitation and inelastic neutron scattering. Fig. 3a shows the expected neutron energy spectra produced in a hadronic shower induced by a 150 GeV pion incident on 9.7λ of iron [Johns K. at II International Conference On Calorimetry in High Energy Physics at TEXAS 1992]. The main conclusions of this simulation study are that:

- The energy spectra sharply cut off at 1 MeV and peak at a few hundred keV ($\approx$ 300 keV), approximately independent of the beam momentum and absorber thickness (Fe).
- The integrated flux decreases by about a factor of 1.6 for each additional λ, see fig. 3b.
- The flux and energy spectrum of albedo neutrons is roughly equal to the flux and energy spectrum of neutrons at 10 λ. For more details see the reference indicated above.

Independent studies [Ferrari CAL-TR-059 and CMS LoI pag. 8] show that there seems to be a very little variation of the neutron fluxes along η in the Barrel calorimeters ($1.5 \leq \eta \leq 0$) for a fixed depth. These references confirm also the neutron flux reduction with the calorimeter depth.

Neutrons produced in the shower will have a large cross section, $\sigma_{elast.}$, to elastically scatter off the protons in the plastic, which constitutes the active medium of the TILECAL calorimeter. At 1 MeV (the maximal energy of the neutron spectra (fig. 3a)) the $\sigma_{elast} \approx \sigma_{tot.}$ is about 4 b (see Appendix A, fig. A.1). The neutron capture in Hydrogen is negligible with respect to the elastic scattering in the full energy range ($\sigma_{n,\gamma} \approx 0.3$ b for thermal neutrons and ≈ 30 μb at 14 MeV (table A.1).

A relation between an integrated neutron fluence F_n (n/cm^2) and the induced dose deposited in the plastic (Gy) considering only elastic processes (σ_{elast} in cm^2) is given by [D. Green FERMILAB-FN-597]:

$$(\text{Dose})_n = F_n \frac{N_O\, \sigma_{elast}}{A} \frac{\langle E \rangle}{2} \qquad (1)$$

where N_O is the number of protons per mass unit ($N_O = 5.2 \times 10^{25} \text{kg}^{-1}$ in the plastic), A is the atomic number of the nucleus on which the neutron is elastically scattered (A = 1 for the free protons in plastic scintillator) and $\langle E \rangle/2$ is the mean energy (in J) of the proton recoil after elastic scattering.

In the case of a mean medium of Fe/LAr (A>> 1) there is a negligible neutron contribution to the total dose. By consequence we assume that the total amount of the doses given previously for a mean medium (fig. 1, 2 and table 1) are only coming from charged particles.

Experimental results of plastic scintillating fibres irradiated with neutrons in a ^{235}U reactor [A. Maio at the LHC Workshop Aachen, Vol. III, pag. 625) have shown that the degradation in both the light emission and light transmission is the same as that from the equivalent dose of γ irradiation (^{60}Co), when similar conversions to eq. 1 are applied to the neutron fluences.

The contribution of neutrons to the doses deposited in the plastic scintillator will be calculated directly from the neutron fluxes expected in the barrel hadron calorimeter. Only the fast (E > 100 keV) fluxes (given in table 1 with a 5 cm polyethylene moderator in front of the LAr e.m. calorimeters, e.g. $1.0x10^{12}$ n/cm^2) were considered. This value is reduced 14% when the LAr is replaced by plastic in the hadron calorimeter [Ferrari EAGLE Internal Note CAL-NO-005]. As discussed later the slow neutrons have a negligible contribution to the dose, and therefore are not taken into account.

For one year running (10^5 pb^{-1}), the expected fast neutron peak flux in the plastic scintillator ((1-0.14)x$1.0x10^{12}$ n/cm^2) corresponds to a peak dose $(Dose)_n$ = 14.7 Gy/y* if we consider <E> = 1 MeV (eq. 1). This assumption overestimates the dose induced by neutrons. This is illustrated in table 2 where the values of $\sigma_{elast.}$ x <E> are given for several neutron energies taken from fig. A.1, note that $Dose_n \propto (\sigma_{elast.} \times <E>)$. For E_n < 1 MeV the contribution of neutrons to the dose decreases considerably. For 300 - 400 keV (the energy at which the neutron flux is maximal) the dose induced by neutrons is reduced to 65% with respect to the dose induced by 1 MeV neutrons, which reduction factor will be taken into account. For smaller neutron energies the corresponding dose will be much smaller (table 2). The contribution of the neutrons with $E_n \leq 100$ keV to the dose is then negligible with respect to the fast neutrons, even if we take into account the fact that the flux of the slow neutrons is about 70% of the total neutron flux in the TILECAL hadron calorimeter with a moderator [Ferrari EAGLE Note CAL-NO-005]. In this study the fluence values used are for E_n > 100 keV.

Neutron energy (MeV)	$\sigma_{elast.}$ x <E> (barn MeV)	Contribution to the dose normalized to 1 MeV
1	4	1
0.3-0.4 (max. flux)	2.8-2.4	0.7-0.6
0.1	1.3	0.33
0.01	0.19	$4.8x10^{-2}$
0.001	0.02	$5x10^{-3}$

Table 2- Values of $\sigma_{elast.}$.<E> for several neutron energies, see fig. A.1..

* *The difference of the doses deposited in the plastic obtained in the ref. [D. Green FERMILAB-FN-597] for the same neutron flux results from the different $\sigma_{elast.}$ used. In this ref. is applied a law of the type $\sigma_{elast} = 7$ barn/E [MeV]$^{0.84}$) which gives $\sigma_{elast.} = 7$ b for 1 MeV neutron instead of 4 b (see fig. A.1c of appendix A).*

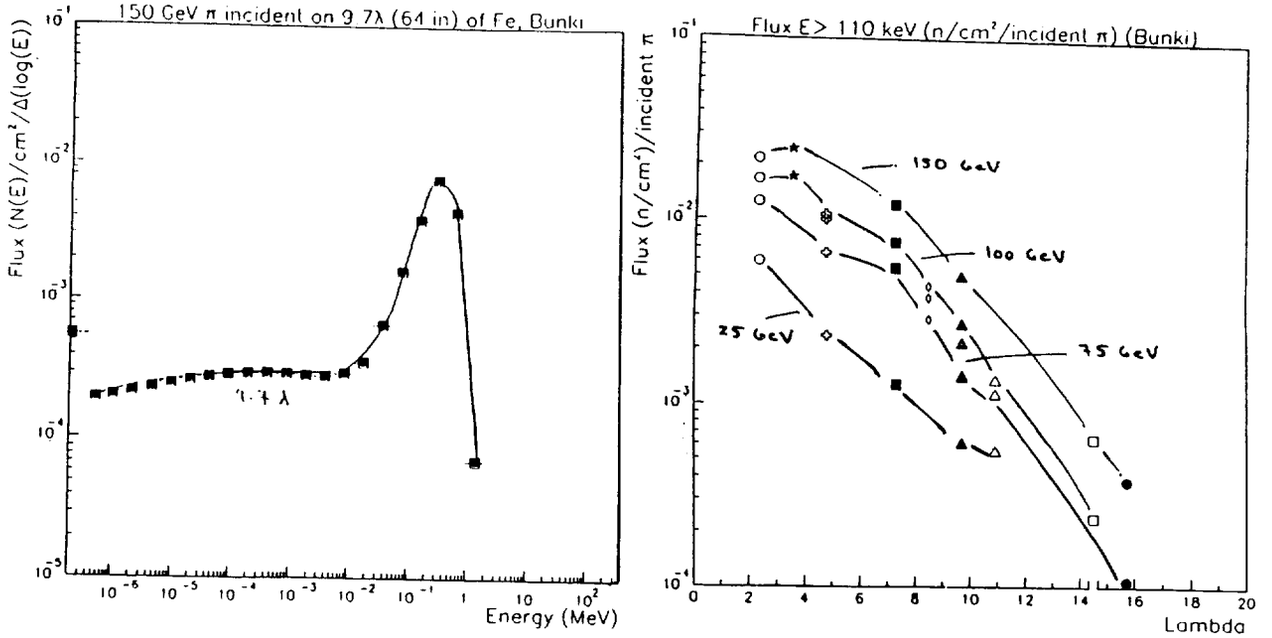

Fig. 3- a) Expected neutron energy spectra produced in a hadronic shower induced by a 150 GeV pion incident on 9.7λ of iron, (b) Expected neutron flux (En > 110 keV) per incident pion of 25 GeV≤ E_π ≤ 150 GeV as a function of the Iron calorimeter depth [Johns K. at II International Conference On Calorimetry in High Energy Physics at TEXAS 1992].

Corrections applied to the doses induced by charged particles and π^0's.

In a iron/plastic scintillator calorimeter with a ratio of 4 to 1, the dose deposited in the plastic by charged particles ($\pi^{\pm}$'s) is higher than the values given for a mean medium of Fe/LAr by a factor roughly proportional to $(dE/dx_{scint}/dE/dx_{<Fe/LAr>} \approx (dE/dx_{scint}/dE/dx_{Fe}. \approx 1.3$. To be conservative we keep the total amount of the doses given previously for a mean medium (fig. 1,2 and table 1) assuming that they are only coming from charged particles. The peak doses in the active medium of the TILECAL hadron calorimeter induced by charged particles are then 11.7 Gy/y and 23.4 Gy/y for $\eta = 0$ and $\eta = 1.5$ respectively.

Final Doses after 10 years working at a peak luminosity of $1.6x10^{34}cm^{-2}s^{-1}$.

For an integrated luminosity of $10^6 pb^{-1}$ (10 years working at a peak luminosity of $1.6x10^{34}cm^{-2}s^{-1}$) the expected peak doses from charged particles, neutrons and the total doses (n + π's) deposited in the plastic scintillator of the TILECAL hadron calorimeter are given on table 3a for $\eta = 0$ and $\eta = 1.5$ with rather conservative assumptions. The variation of the doses with the hadronic calorimeter depth are shown on table 3b and fig. 4.

Peak doses in the active medium of the Barrel TILECAL Calorimeter after $10^6 pb^{-1}$			
η	Dose from charged part. (Gy)	Dose from neutrons (Gy)	Total Dose (Gy)
0	117	96 (–>0.56 x 10^{13} n/cm^2)	264
1.5	234	96 (–>0.56 x 10^{13} n/cm^2)	381

Table 3a - Peak doses (Gy) expected in the plastic scintillator of the had. calorimeter from charged particles and neutrons after an integrated luminosity of $10^6 pb^{-1}$, for $\eta = 0$ and $\eta = 1.5$, see details in text.

Doses versus the depth of the TILECAL Calorimeter after $10^6 pb^{-1}$				
η	Depth (λ units)	Dose from charged particles (Gy)	Dose from neutrons (Gy)	Total Dose (n + π's) (Gy)
0	1.95	129.99	95.56	225.55
	2.46	80.15	44.76	124.91
	2.96	46.93	26.62	73.55
	3.55	26.04	17.91	43.95
	4.21	12.64	12.83	25.48
	4.87	6.30	9.57	15.87
	5.61	2.90	6.97	9.87
	6.42	1.23	4.95	6.18
	7.23	0.52	3.51	4.04
	8.17	0.19	2.36	2.56
	9.24	0.06	1.50	1.56
	10.31	0.02	0.96	0.98
1.5	1.95	259.97	95.56	355.54
	2.46	117.99	44.76	162.75
	2.96	91.769	26.62	118.39
	3.55	65.55	17.91	83.46
	4.21	26.22	12.83	39.05
	4.87	20.98	9.57	30.54
	5.61	14.42	6.97	21.39
	6.42	9.59	4.95	14.53
	7.23	7.87	3.51	11.38
	8.17	5.24	2.36	7.61
	9.24	3.67	1.50	5.18
	10.31	2.10	0.96	3.06

Table 3b- Doses (Gy) expected in the plastic scintillator of the TILECAL hadron calorimeter as a function of the calorimeter depth after an integrated luminosity of $10^6 pb^{-1}$, for $\eta = 0$ and $\eta = 1.5$. Doses are given for charged particles, neutrons and the total doses (neutrons and charged particles). It is assumed that the neutron fluxes given by Ferrari in the ATLAS configuration (at $\eta = 1.5$) remain the same for $\eta = 0$, for a certain depth, and decreases by a factor of 10 after every 5 λ, see text for details.

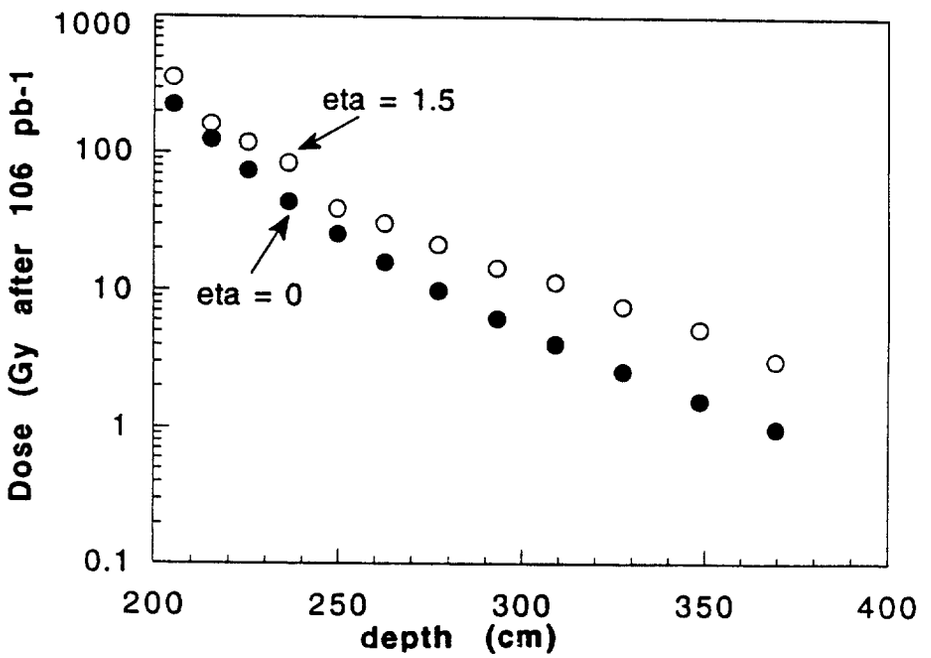

Fig. 4- Total doses (neutrons and charged particles) in Gy expected in the had. calorimeter after an integrated luminosity of $10^6 pb^{-1}$ for $\eta = 0$ and $\eta = 1.5$, as a function of the hadron calorimeter radial depth.

II) Radiation Hardness of a Tile/WLS fibre calorimeter

To evaluate the light reduction as a function of the dose, the SDC experimental radiation damage results were used, since this is the closest configuration to the TILECAL calorimeter. Intensive tests were performed irradiating in electron beams and γ- ^{60}Co sources several test modules filled with different tile/fibre combinations [SDC technical proposal (SDC-92-201, pag. 6-31 ; Rad. Phys. Chem. Vol 41, 1993, pag. 263, etc.]. We have chosen experimental results of a typical combination tile/fibre module with a good compromise between a high light yield before irradiation and a good radiation hardness, which is a blue plate SCSN81 combined with a green Y7 fibre* , both from Kuraray. In fig. 5 [SDC-92-201, pag. 6-367 and Yasuoka at the TEXAS calorimetry conference September 1992] is shown the light ratio as a function of the dose in Mrad (1Gy = 100 rad) at the maximum of the shower induced by 2.5 GeV electrons in a SDC module filled with SCSN38/Y7 combination. The data from 3 different modules fit well with a 2 exponential curve:

$$I/I_0 = 0.824\ e^{-D/\gamma 1} + 0.157\ e^{-D/\gamma 2} \qquad (2)$$

With γ_1 = 4.3 Mrad (= 43000 Gy) and γ_2 = 0.135 Mrad (= 1350 Gy). With this fit a 1.9% permanent light reduction is given for a zero dose, which was not removed to infer the light reduction after a certain dose. This data were obtained with 11x11 cm^2 plates with 3 mm thickness. Tests have also been done comparing the effect of damage on short and long plates. In fig. 6 [Yasuoka at the TEXAS calorimetry conference, October 1992] a transverse uniformity scan is shown before and after

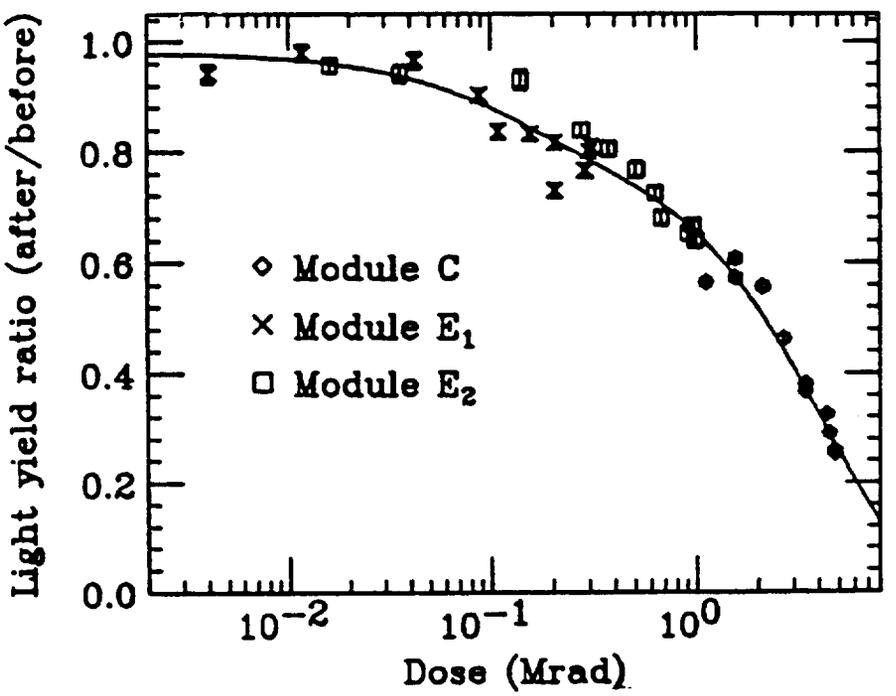

Fig. 5- Light yield ratio after irradiation at shower maximum for SCSN81/Y7 modules as a function of the dose at the shower maximum.

---

* *The BCF91A fibre presently used in the TILECAL test modules has similar radiation hardness when compared with the Y7 fibre type [Yasuoka at the TEXAS calorimetry conference September 1992].*

irradiating a plate/fiber (SCSN81//Y7 fibre) assembly (not a module) in a ^{60}Co source to 0.6 Mrad (6 kGy). The results are given for a short and long tile of 10.5x10.5 cm^2 and 10.5x22.5 cm^2 respectively, showing a negligible difference between the two plates, within the error bars.

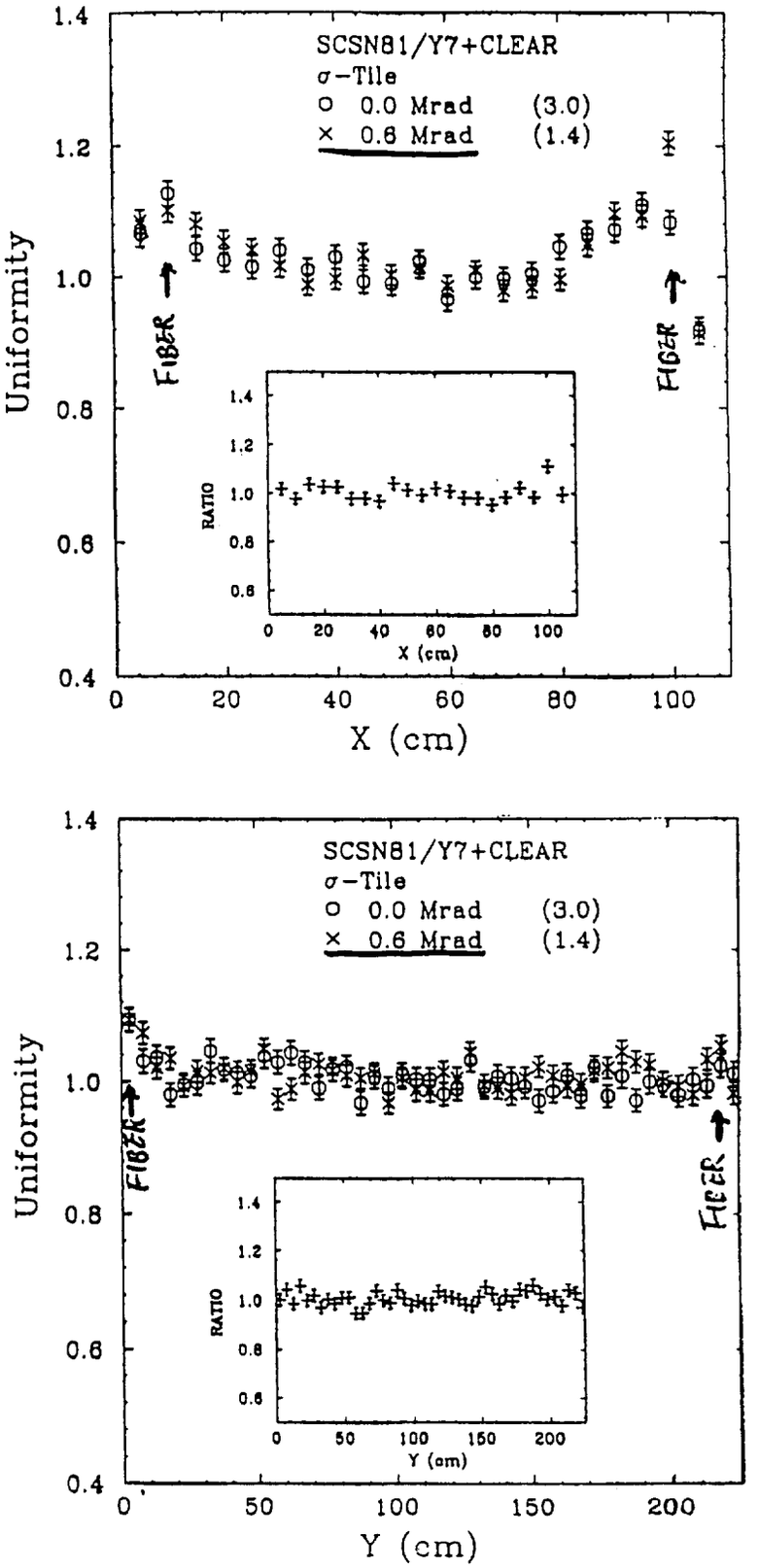

Fig. 6 Transverse uniformity for two tile size of 10.5x10.5 cm^2 and 10.5x22.5 cm^2 after and before irradiation uniformly in a ^{60}Co source [Yasuoka at the TEXAS conference, October 1992].

a) Expected light ratio in the Barrel at $\eta = 0$ after $10^6 pb^{-1}$		
Tile Number	Light Yield ratio (%)	Light yield ratio (%) after calibrating each of the 4 sectors
1	95.25	98.93
2	96.47	1.00
3	97.13	1.00
4	97.51	99.79
5	97.76	1.00
6	97.89	1.00
7	97.97	99.97
8	98.02	1.00
9	98.05	1.00
10	98.07	99.99
11	98.08	1.00
12	98.09	1.00
b) Expected light ratio in the Barrel at $\eta = 1.5$ after $10^6 pb^{-1}$		
Tile Number	Light Yield ratio (%)	Light yield ratio (%) after calibrating each of the 4 sectors
1	93.79	98.26
2	96.00	1.00
3	96.56	1.01
4	97.00	99.57
5	97.58	1.00
6	97.69	1.00
7	97.81	99.92
8	97.90	1.00
9	97.95	1.00
10	98.00	99.97
11	98.03	1.00
12	98.06	1.00

Table 4- Expect light yield ratio in each tile of the barrel hadron calorimeter after an integrated luminosity of $10^6 pb^{-1}$ (a) for $\eta = 0$ and (b) $\eta = 1.5$. The last columns gives the light ratio after calibrating each of the 4 longitudinal sectors. The mean of the light given in each of the sector formed by 3 plates was used to calibrate.

Due to the absence of experimental results concerning irradiation in the exact TILECAL configuration, the results of fig. 5 have been used in this study, to be considered the closest to our case. Using eq. 2 and the results of fig. 4 we estimated the light yield ratio expected on the hadron calorimeter for $\eta = 0$ and $\eta = 1.5$ after an integrated luminosity of $10^6 pb^{-1}$. The results are shown on table 4 and fig. 7. We observe that before recalibrating longitudinally each of the 4 cells the light reduction in the first tile (the worst case) is 4.8% for $\eta = 0$ and 6.2% for $\eta = 1.5$. Assuming that it is possible to know the longitudinal profile of the damage, each of the four longitudinal sectors can be calibrated. The results obtained are given on the last column of table 4a,b. The light ratio in the first tile deviates by 1.1% and 1.8% from the calibration constant in the first sector for $\eta = 0$ and for $\eta = 1.5$ respectively.

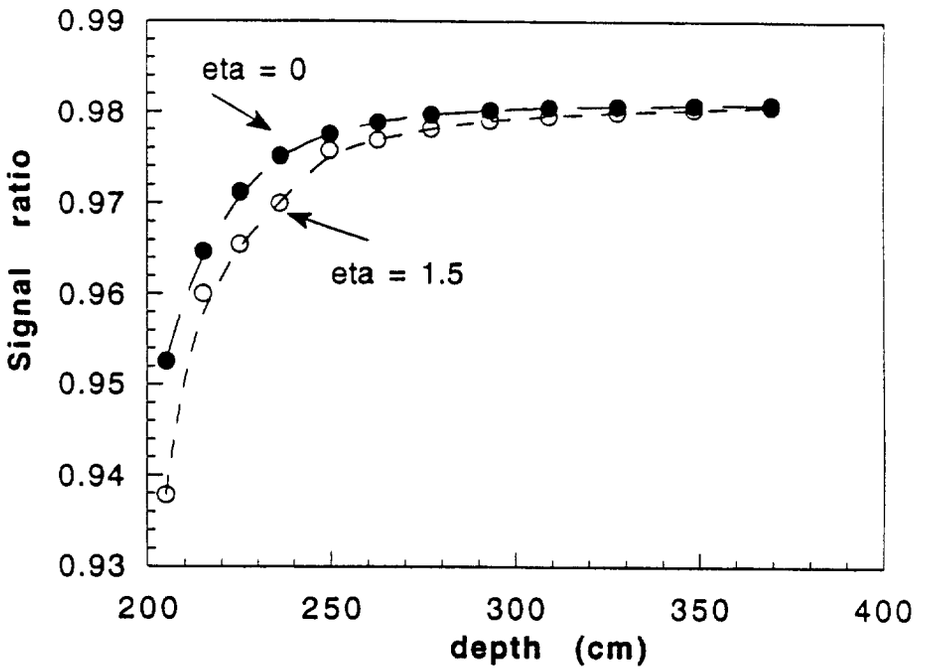

Fig. 7- Effect of the irradiation on the light ratio (%) of the TILECAL calorimeter as a function of the depth after an integrated luminosity of $10^6 pb^{-1}$. This includes the effect of neutrons and charged particles deposited in the plastic scintillator.

III) Effect of Radiation Damage on the Performance of the TILECAL hadron calorimeter in the Barrel region.

Jets of 300 GeV have been generated using GEANT and FLUKA in the ATLAS configuration (Accordion Lar/Pb e.m. and TILECAL had. calorimeter), at $\eta = 0$. The effect of radiation to the jet energy resolution has been studied. The results of table 4a,b have being used giving to each cell a different weight in order to reproduce the light ratio of each tile after $10^6 pb^{-1}$, either at $\eta = 0$ or $\eta = 1.5$. In the e.m. calorimeter no degradation due to radiation was considered. Fig. 8 shows the signal distribution for 300 GeV jets at $\eta = 0$ (a) before irradiation, (b) after irradiation but without calibration, and (c) after longitudinal calibration. The effect of radiation if we considered the doses expected at $\eta = 1.5$ is shown in fig. 9.

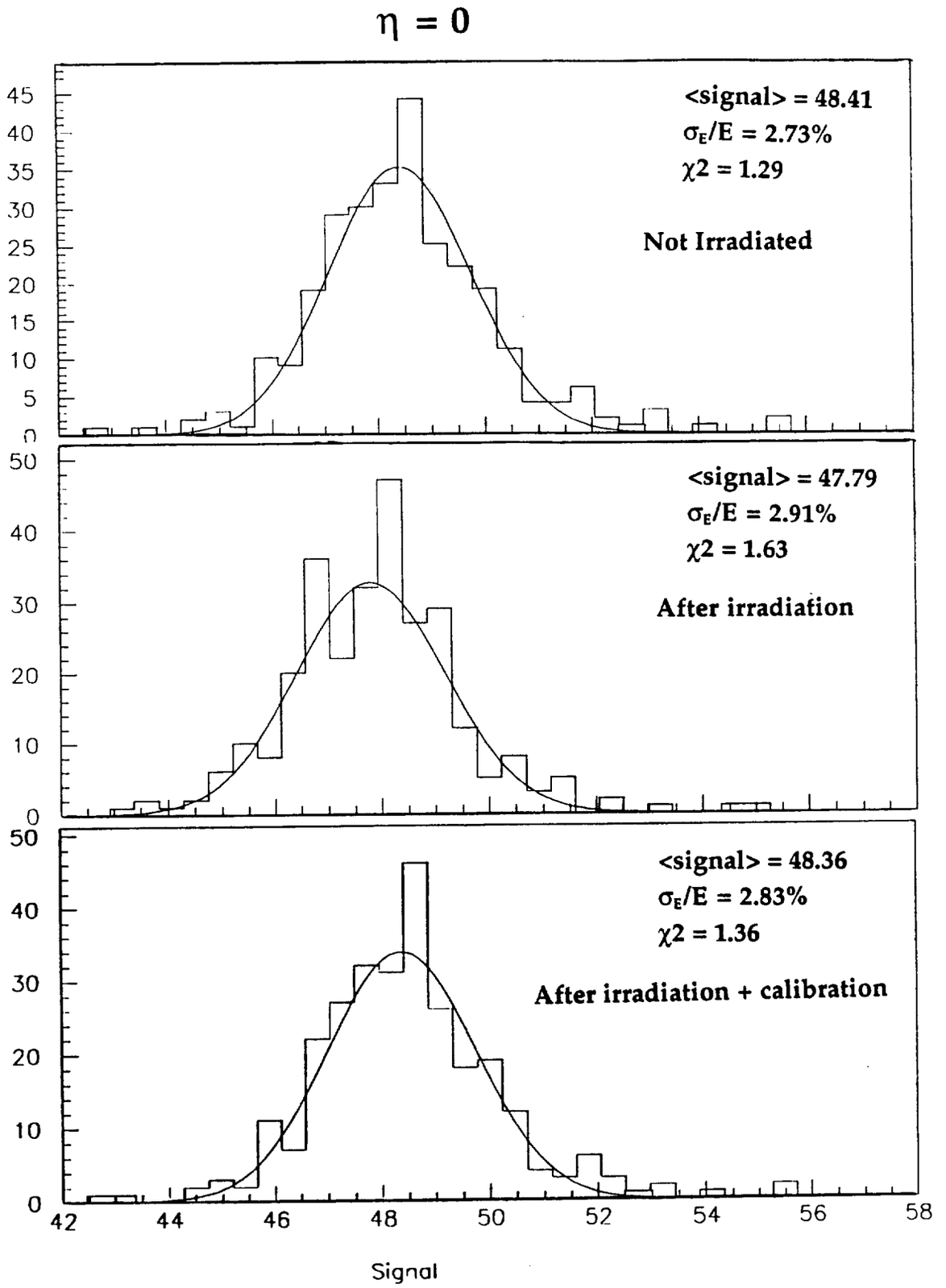

Fig. 8- The signal distribution for 300 GeV jets generated at η = 0 (a) before irradiation, (b) after irradiation with the doses expected at η = 0, but without longitudinal calibration, and (c) after longitudinal calibration. It was considered the effect after $10^6 pb^{-1}$.

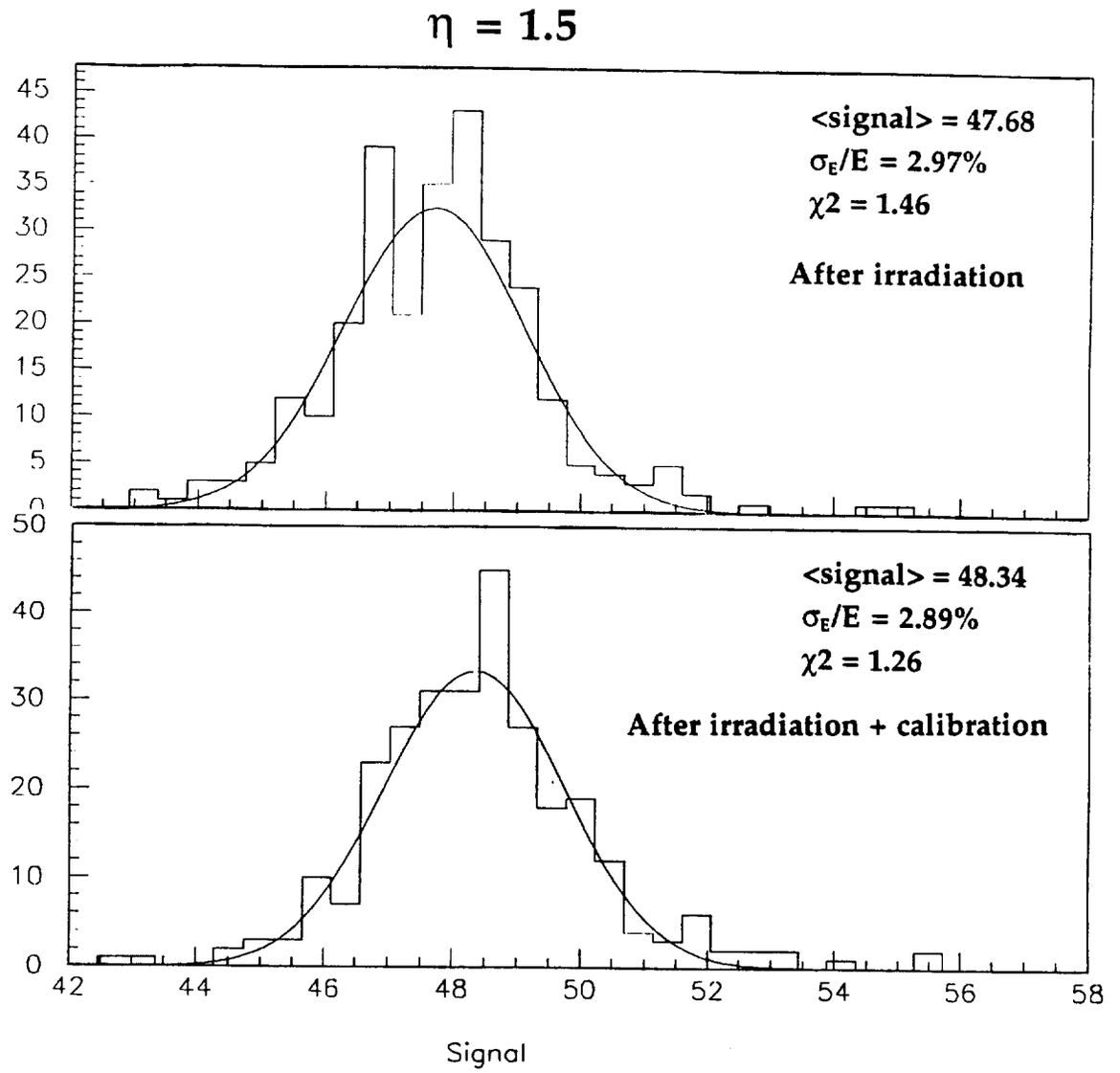

Fig. 9- The signal distribution for 300 GeV jets generated at η = 0 (a) after irradiation with the doses expected at η = 1.5, but without longitudinal calibration, and (b) after longitudinal calibration. It was considered the effect after $10^6 pb^{-1}$.

We observe that even at η = 1.5 and without longitudinal calibration the effect of radiation on the jet energy resolution is marginal, as well as in the light reduction. In table 5 are given the values of the increase of the jet energy resolution and light reduction both at η = 0 and η =1.5.

	η = o		η = 1.5	
	Increase on $\sigma_{E/E}$ (%)	Signal reduction (%)	Increase on $\sigma_{E/E}$ (%)	Signal reduction (%)
without calibration	0.18	1.28	0.24	1.51
after calibration	0.10	0.10	0.16	0.14

Table 5- Expected degradation of the TILECAL hadron calorimeter performance in the ATLAS configuration obtained by generating 300 GeV jets with GEANT and FLUKA. The values given are for an integrated luminosity of $10^6 pb^{-1}$.

Appendix A

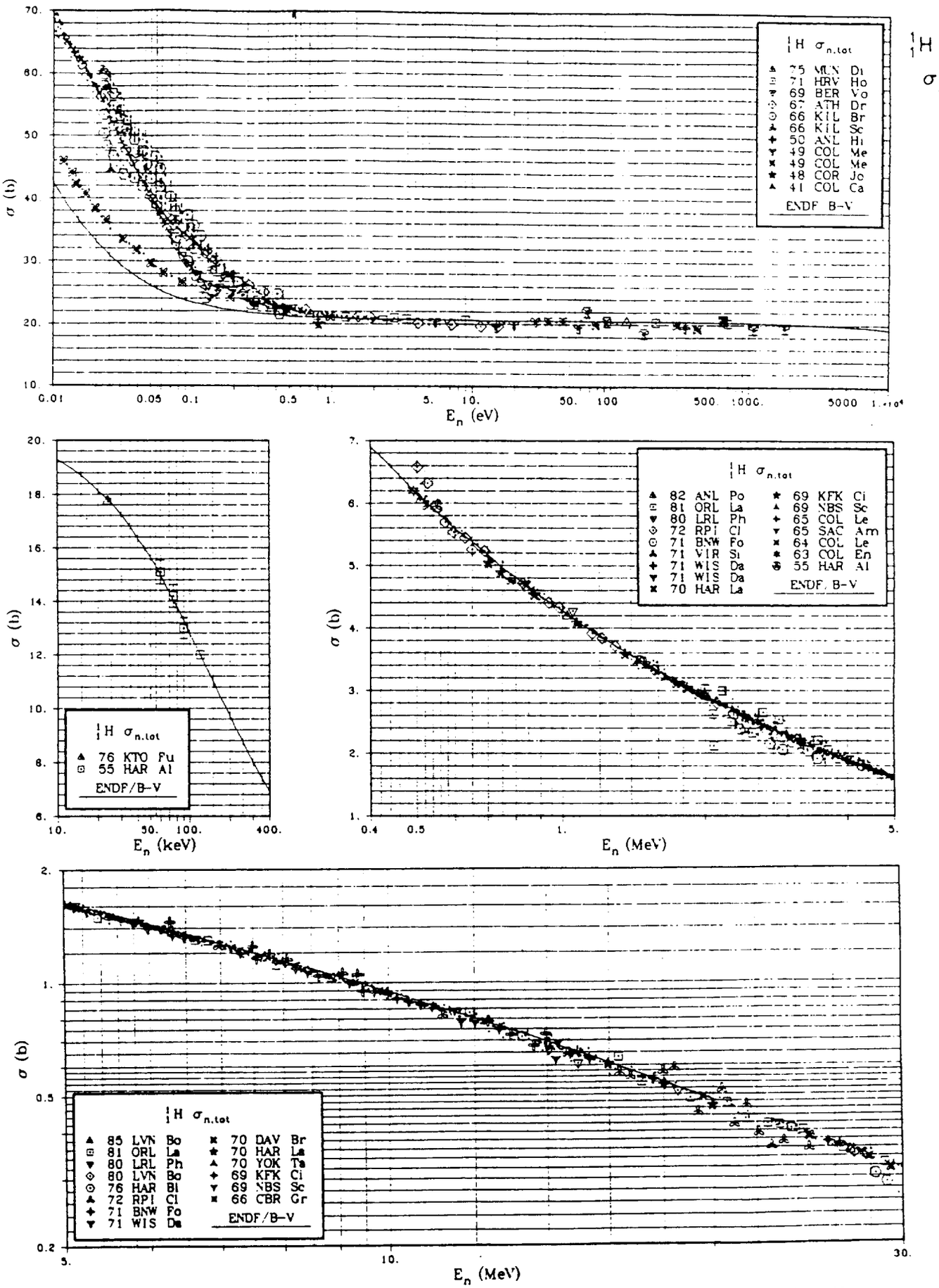

Fig. A.1- Neutron cross sections curves [Neutron cross section curves, volI, Academic press, Inc. Harcourt Brace Jovanovich, Publishers].

Yr	Lab	Author	Reference	Points	Range			Standard	
					^1_1H $\sigma_{n,\gamma}$				
85	BLG	Dupont+	NP/A 445, 13	5	45.00 MeV	to	70.00 MeV		
85	ROS	Stiehler+	PL/B 151, 185	1	26.60 μb	at	25.00 MeV	^{1}H	$\sigma_{n,el}$
80	CAB	Lolich+	AKE 35 (1), 23	1	0.329 b	at	thermal		
79	LVN	Bosman+	PL/B 82 2, 212	7	37.00 MeV	to	72.60 MeV	^{1}H	$\frac{d\sigma_{n,el}}{d\Omega}$
77	COL	Cokinos+	PR/C 15, 1636	1	0.333 b	at	thermal		
69	UJV	Bayer+	CZJ/B 19, 911	1	0.336 b	at	thermal		
67	RBZ	Tudoric	NP/A 92, 233	1	30.60 μb	at	14.40 MeV		
65	KFI	Pal+	65KRLSRH 1 (98), 165	1	0.333 b	at	thermal		
65	OXF	Cox+	NP 74, 497	1	0.334 b	at	thermal		
64	RBZ	Slaus+	64PARIS 2, 244	1	33.80 μb	at	14.40 MeV		
62	UJV	Dlouhy+	JNE/AB 16, 376	2	25.30 mv	to	25.30 mv		
61	ANL	Meadows+	NSE 9, 132	1	0.335 b	at	thermal		
61	RBZ	Cerineo+	PR 124 (6), 1947	1	31.60 μb	at	14.40 MeV	^{1}H	$\sigma_{n,el}$
61	UJV	Bayer+	CZJ/A 11, 480	1	0.335 b	at	thermal		
58	HAR	Baker	PRS/A 248, 539	1	0.327 b	at	thermal	B	$\sigma_{n,abs}$
45	UI	Schulz+	PR 67, 202(E2)	1	0.307 b	at	thermal	B	$\sigma_{n,\gamma}$
38	MHG	Spees+	PR 53, 326(20)	1	0.260 b	at	thermal	Cd	$\sigma_{n,\gamma}$
					^2_1H $\sigma_{n,tot}$				
80	LRL	Phillips+	PR/C 22, 384	71	71.00 keV	to	43.44 MeV		
79	NIL	Gul+	79KNOX, 39(AB2)	1	0.765 b	at	14.80 MeV		
75	HRV	Callerame+	PR/C 12, 1428	1	16.80 b	at	4.200 mv		
73	RPI	Stoler+	PR/C 8, 1539	446	22.40 keV	to	0.993 MeV		
72	DAV	Brady+	PR/C 6, 1150	8	24.63 MeV	to	59.35 MeV		
72	RPI	Clement+	NP/A 183, 51	432	0.501 MeV	to	29.91 MeV		
72	YOK	Koori	JPJ 32, 306	1	0.809 b	at	14.10 MeV		
71	WIS	Davis+	PR/C 3, 1798	27	1.500 MeV	to	27.52 MeV		
66	HRV	Measday+	NP 85, 142	7	88.20 MeV	to	0.151 GeV		
65	HAR	Riddle+	NP 61, 457	28	17.50 MeV	to	0.113 GeV		
64	ORL	Willard+	PL 9, 339	31	2.790 MeV	to	3.570 MeV		
60	LRL	Peterson+	PR 120, 521	4	17.80 MeV	to	29.00 MeV		
58	LRL	Bratenahl+	PR 110, 927	5	7.160 MeV	to	14.01 MeV		
55	HRV	Culler+	PR 99, 740	4	93.40 MeV	to	0.107 GeV		
55	LAS	Seagrave+	PR 98, 666	29	0.267 MeV	to	21.85 MeV		
54	RIC	Cook+	PR 94, 651	8	14.10 MeV	to	18.00 MeV		
53	MIT	Zimmerman+	PR 90, 339(C5)	4	0.100 MeV	to	1.320 MeV		
53	WIS	Adair+	PR 89, 1165	9	0.262 MeV	to	2.962 MeV		
52	ANL	Goodman	PR 88, 686	1	0.820 b	at	14.00 MeV		
52	BNL	Poss+	PR 87, 11	1	0.803 b	at	14.10 MeV		
51	LAS	Meyer+	LA-1279	1	0.810 b	at	14.20 MeV		
50	BRK	Hildebrand+	PR 80, 842	1	0.289 b	at	42.00 MeV		
50	BRK	De Juren+	PR 77, 606	1	0.104 b	at	95.00 MeV		
49	BRK	Cook+	PR 75, 7	1	0.117 b	at	83.00 MeV		
46	MIN	Nuckolls+	PR 70, 805	15	0.350 MeV	to	6.000 MeV		
39	COL	Zinn+	PR 56, 260	1	2.170 b	at	2.880 MeV		
					^2_1H $\sigma_{n,el}$				
83	KFK	Schwarz+	NP/A 398 (1), 1	20	2.500 MeV	to	30.00 MeV	^{1}H	$\frac{d\sigma_{n,el}}{d\Omega}$
79	NEU	Chatelain+	NP/A 319 1, 71	2	2.480 MeV	to	3.270 MeV	^{2}H	$\frac{d\sigma_{n,el}}{d\Omega}$
79	NIL	Gul+	79KNOX, 39(AB2)	1	0.620 b	at	14.80 MeV		
72	LAS	Seagrave+	AP 74, 250	8	5.550 MeV	to	23.00 MeV		
72	YOK	Koori	JPJ 32, 306	1	0.826 b	at	14.10 MeV		
70	DAV	Romero+	PR/C 2, 2134	2	36.00 MeV	to	46.30 MeV	^{1}H	$\frac{d\sigma_{n,el}}{d\Omega}$
68	CLA	Berick+	PR 174, 1105	1	0.650 b	at	14.30 MeV	H	$\sigma_{n,tot}$
68	ETH	Bruellmann+	HPA 41, 435	1	0.650 b	at	14.14 MeV	^{1}H	$\sigma_{n,el}$
66	TOU	Vedrenne	JPR/C 27 (1), 71	1	0.607 b	at	14.10 MeV	^{1}H	$\sigma_{n,el}$
55	HAR	Allen+	PPS/A 68, 650	3	0.100 MeV	to	0.200 MeV	^{1}H	$\sigma_{n,el}$
55	LAS	Seagrave	PR 97, 757	1	0.610 b	at	14.10 MeV		
53	HAR	Tunnicliffe	PR 89, 1247	8	0.135 MeV	to	0.914 MeV	^{1}H	$\sigma_{n,el}$
53	LAS	Allred+	PR 91, 90	1	0.670 b	at	14.10 MeV		

Table A.1- Neutron cross section values in Hydrogen [Neutron cross section curves, voll, Academic press, Inc. Harcourt Brace Jovanovich, Publishers].